

Self-Similarity and Universality in Rayleigh-Taylor, Boussinesq Turbulence

Natalia Vladimirova*

ASC Flash Center, The University of Chicago, Chicago, IL 60637[†]

Michael Chertkov[‡]

CNLS and T-13, Theory Division, Los Alamos National Laboratory, Los Alamos, NM 87544

We report and discuss case study simulations of the Rayleigh-Taylor instability in the Boussinesq, incompressible regime developed to turbulence. Our main focus is on a statistical analysis of density and velocity fluctuations inside of the already developed and growing in size mixing zone. Novel observations reported in the article concern self-similarity of the velocity and density fluctuations spectra inside of the mixing zone snapshot, independence of the spectra of the horizontal slice level, and universality showing itself in a virtual independence of the internal structure of the mixing zone, measured in the re-scaled spatial units, of the initial interface perturbations.

Keywords: turbulence — mixing zone — scale-separation — self-similarity — universality

I. INTRODUCTION

The Rayleigh-Taylor instability occurs when a heavy fluid is being pushed by a light fluid. Two plane-parallel layers of fluid, colder on top, are in equilibrium while the slightest perturbation leads to the denser fluid moving down and the lighter material being displaced upwards. The early, linear stage of the instability was described by Rayleigh [1] and Taylor [2], and summarized in [3]. Further development of the instability leads to enhancement of the mixing and to a gradual increase of the mixing zone, which is the domain where proportions of heavy in light and light in heavy are comparable. Dimensional arguments, supported by large-scale modeling [4, 5], suggest that the half-width of the mixing zone, h , grows quadratically at late time, $h \propto \alpha A g t^2$, where A is the Atwood number characterizing the initial density contrast, g is the gravitational acceleration, and α is a dimensionless coefficient.

The coefficient α was the focus of almost every paper written on the subject of Rayleigh-Taylor turbulence (RTT) during the last fifty years. The first attempts to look inside the mixing zone were initiated only in late 1990s [6, 7, 8], due to advances in experimental and numerical techniques. The results of many studies and the controversies surrounding the α -coefficient were recently summarized in the review combining and analyzing the majority of existing α -testing simulations and experiments [9]. In this article we also discuss the developed regime of RT turbulence. Our main focus is on the analysis of the internal structure of the mixing zone, and we trace the α -coefficient only for validation purposes.

Our analysis of the mixing zone develops and ex-

tends previous experimental [6, 10, 12] and numerical [6, 13, 14, 15, 16, 17, 18] observations on the subject, and it is also guided by phenomenological considerations discussed in [19]. The essence of the phenomenology, which utilizes the classical Kolmogorov-41 approach [20], can be summarized in the following statements: (i) The mixing zone width, h , and the energy containing scale, R_0 , are well separated from the viscous, η , and diffusive, r_d , scales. In the inertial range, realized within the asymptotically large range bounded by R_0/η from above/below, turbulence is adjusted adiabatically to the large-scale buoyancy-controlled dynamics. (ii) In three dimensions, the velocity fluctuations at smaller scales are asymptotically decoupled from weaker buoyancy effects [29]. (iii) Typical values of velocity and density fluctuations scale the same way as in the stationary, homogeneous Kolmogorov turbulence, $\delta v_r \sim (\epsilon r)^{1/3}$, and $\delta \rho_r \sim \epsilon_\rho^{1/2} \epsilon^{-1/6} r^{1/3}$, where the energy Kolmogorov flux, ϵ , increases with time while the density fluctuations flux, ϵ_ρ , remains constant, according to the buoyancy prescribed large scale dynamics. All of these three theses of the phenomenology are consistent with available experimental [6, 12] and numerical [13, 14, 18, 22] observations of the velocity and density spectra. One particularly important consequence of the phenomenology, the decrease of the viscous and dissipative scales, was also predicted in [15] and numerically confirmed in [15, 18].

In spite of its relative success in explaining RTT, the phenomenology [19] is, obviously, not free from deficiencies. First, the asymptotic, large time character of the theory turns into a handicap in explaining numerical and experimental data, taken at finite, and actually modest, times. Second, the phenomenology treats all z -slices within the mixing zone equally. Third, the phenomenology does not differentiate between the mixing zone width, h , and the energy containing scale, R_0 , for the turbulent fluctuations.

Improving the phenomenology from within itself, or by some complementary theoretical means, does not

*Electronic address: nata@flash.uchicago.edu

[†]also at CNLS and T-13, Theory Division, Los Alamos National Laboratory, Los Alamos, NM 87544

[‡]Electronic address: chertkov@lanl.gov

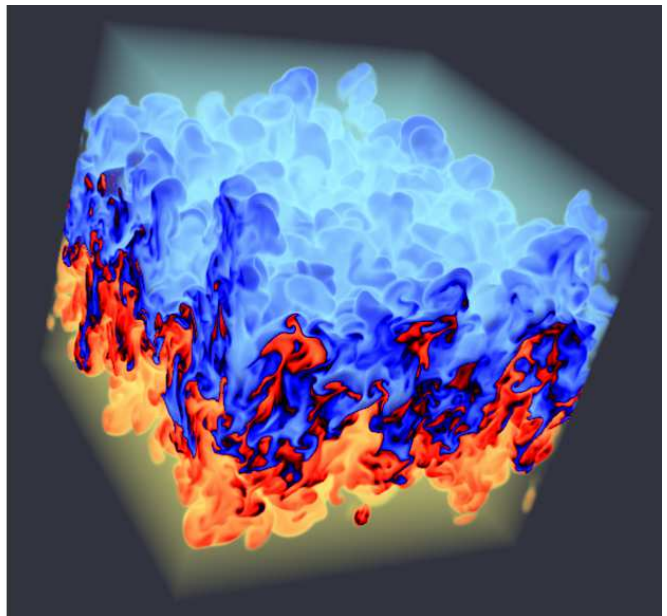
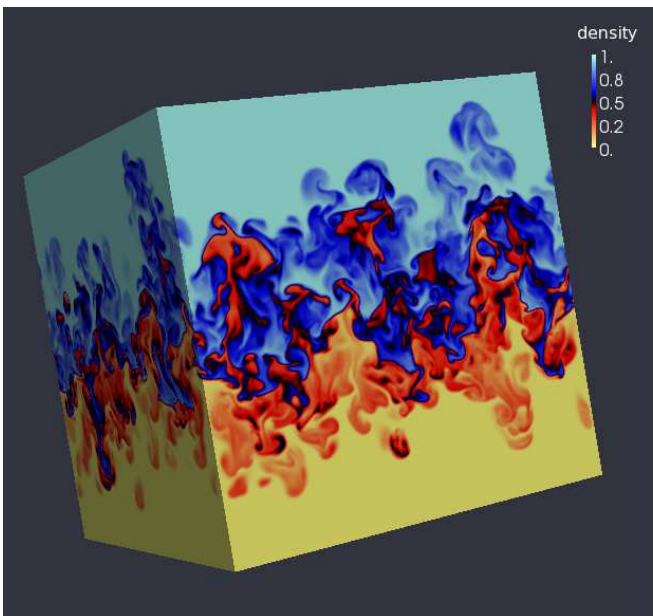


FIG. 1: Density at $t = 128$ in the simulation with narrow initial spectrum in 960^3 domain.

seem feasible, and one needs to rely on resolving these questions/uncertainties through experiments and simulations. This article reports a step in this direction. Here we raise and give partial answers, based on simulations, to the following subset of key questions concerning the internal structure of the RTT mixing zone:

- Analyzing the evolution of h , R_0 , r_d and η with time one often observes a non-universal, simulation/experiment specific behavior, especially at transient, so-called early self-similarity, times [15]. Will the relative dependence of scales be a more reliable indicator of a universal behavior than the time-dependence of the scales?
- How does the energy containing scale, R_0 , compare with the width of the mixing layer, h ? This question was already addressed in [15]. Here, we will elaborate on this point.
- How different are the turbulent spectra at different vertical positions in the mixing zone within a given time snapshot?
- How different are the scales and spectra corresponding to qualitatively different initial perturbations?

The material in this article is organized as follows. We start by describing our simulations, we then proceed to the definitions and subsequently the observations of the various spatial scales characterizing snapshots of the mixing zone. Finally we discuss self-similarity and universality of the emerging spatio-temporal picture of the RTT. We conclude by answering the questions posed above.

II. DESCRIPTION OF SIMULATIONS

We consider 3D incompressible, miscible Rayleigh-Taylor flow in the Boussinesq regime,

$$\begin{aligned} \partial_t \mathbf{v} + (\mathbf{v} \cdot \nabla) \mathbf{v} + \nabla p - \nu \Delta \mathbf{v} &= Agc, & \nabla \cdot \mathbf{v} &= 0, & (1) \\ \partial_t c + (\mathbf{v} \cdot \nabla) c &= \kappa \Delta c, & & & (2) \end{aligned}$$

where κ and ν are the diffusion and viscosity coefficients, while $c = (\rho - \rho_{\min})/(\rho_{\max} - \rho_{\min})$ is the normalized density. The Boussinesq approximation for gravity corresponds to fluids with small density contrast, $A \ll 1$, where $A = (\rho_{\max} - \rho_{\min})/(\rho_{\max} + \rho_{\min})$ is the Atwood number. Here, we restrict ourself to the case of $\kappa = \nu$.

We solve equations (1-2) using the spectral element code of Fischer et al [23] designed specifically for DNS of Boussinesq fluids. The equations are solved in the nondimensional units,

$$[l] = (2Ag)^{-\frac{1}{3}} \nu^{\frac{2}{3}}, \quad [t] = (2Ag)^{-\frac{2}{3}} \nu^{\frac{1}{3}};$$

the results are presented in the same units. This choice of units is based solely on the dimensional parameters in Eqs. (1-2) thus reflecting free boundary conditions (absence of any wall constraints). The critical wavelength and the wavelength of the linearly most unstable mode are constants in these units.

The boundary conditions are periodic in the horizontal directions and no-slip in vertical direction. The initial conditions include a quiescent velocity and a slightly perturbed interface between the layers, $c(t = 0; z) = -\theta(z + \delta(x, y))$, where $\theta(z) = \frac{1}{2}[1 - \tanh(0.4z)]$ is the function describing the density profile across the interface and $\delta(x, y)$ is the perturbation.

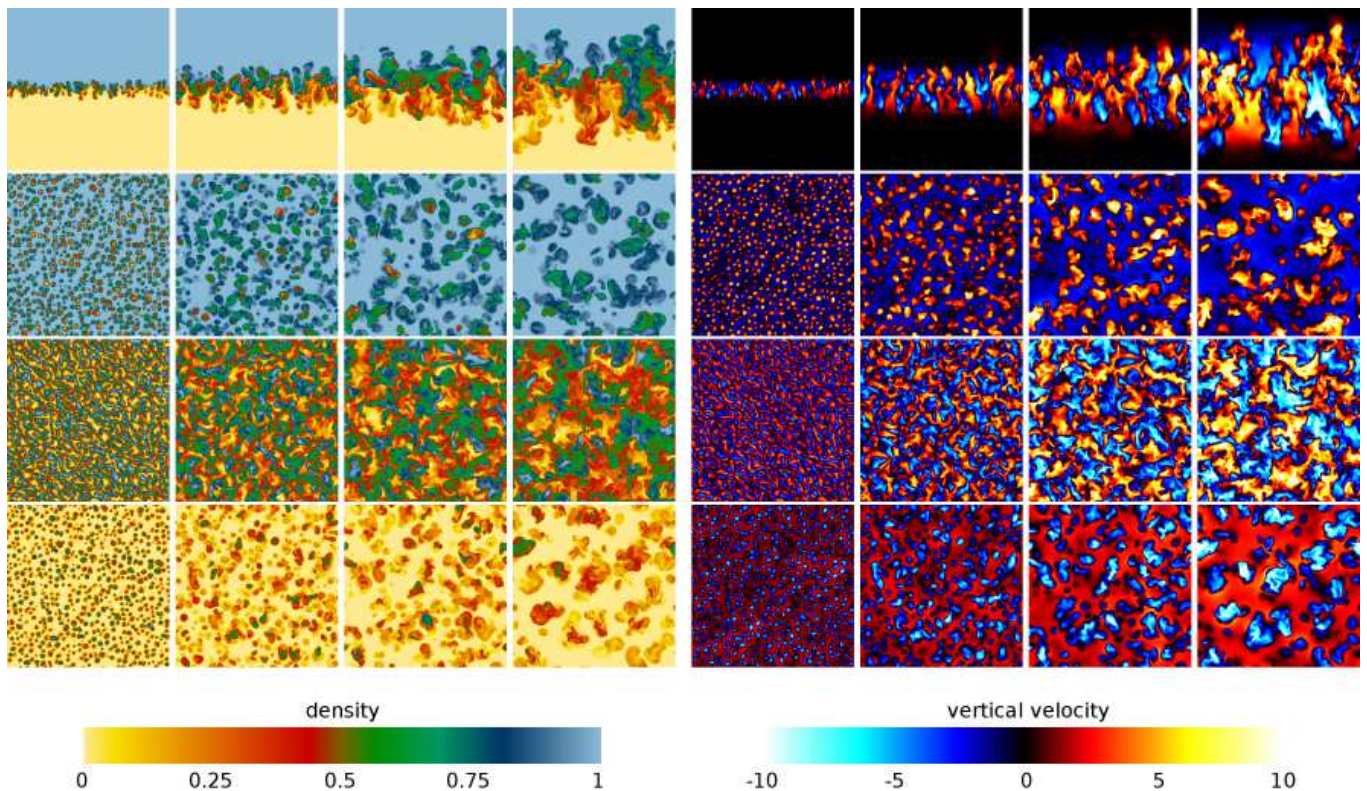


FIG. 2: Slices of density and vertical velocity at times $t = 32, 64, 96, 128$ (left to right) in simulation with narrow initial spectrum in 960^3 domain; from top to bottom, the images correspond to vertical slice at $y = 480$ and horizontal slices at $z = +0.75h, 0, -0.75h$.

We use spectral elements of size 30^3 with 12 collocation points in each direction. This is equivalent to the spectral resolution with the spacing between points $\Delta = 3$. The size of our largest computational domain is $1920 \times 1920 \times 1440$ physical units, or $768 \times 768 \times 576$ collocation points. We stop our simulation at, $t = 128$, when the width of the mixing layer reaches the domain size. At the end of simulation, the Reynolds number reaches $\mathfrak{R} = 7500$ to $\mathfrak{R} = 13000$ depending on the initial conditions, where $\mathfrak{R} = \frac{4h\bar{h}}{\nu}$. For comparison, the largest Rayleigh-Taylor simulation to date [18] was performed in a 3096^3 domain at resolution $\Delta = 1$ and reaching time $t = 248$ and $\mathfrak{R} = 30000$. Our relatively coarse resolution might raise concerns, especially in diagnostics of small structures. Nevertheless, all our results, including the spectra and the estimates for microscale η , are in a very good agreement with [18], as well as with our finer-resolved (but smaller) simulation with $\Delta = 1$.

In all cases studied, the (initial) fastest growing mode is located at $\lambda \approx 24$. Most of the presented results were obtained in the simulations in the domain of $1920 \times 1920 \times 1440$ physical units with initial perturbation in the form of a narrow initial spectrum, with modes $36 \leq n \leq 96$ and spectral index 0. (Here the spectral index refers to the exponent of the wavenumber, as in [24], and describes the

shapes of the spectra.) To investigate the influence of initial condition we also performed additional simulations in smaller domain of size 960^3 (in physical units) with: (1) a narrower initial spectrum, with modes $18 \leq n \leq 48$ and spectral index 0 (Figure 1); and (2) a broader initial spectrum, with modes $3 \leq n \leq 96$ and spectral index -1 . The two regimes were identified in previous studies as giving distinctly different $h(t)$ at transient times [24]. According to [24], the first system develops a mode-merging regime and exhibits scalings with universal α , while the second system develops in the regime of mode-competition, with α depending on the amplitude of the initial perturbation. We observed that, in spite of the early stage differences, the additional simulations gave the same results in the turbulent (advanced time) regime as the main set.

One important focus of our simulations/analysis is on resolving the vertical inhomogeneity of the mixing zone (Figure 2). To achieve this goal we differentiate vertical slices within a given snapshot, thus calculating various characteristics of the mixing zone such as the energy containing scale, the energy spectra and the viscous scale. We collect statistics within a given slice z , e.g. contrasting results for the mixing zone center and its periphery.

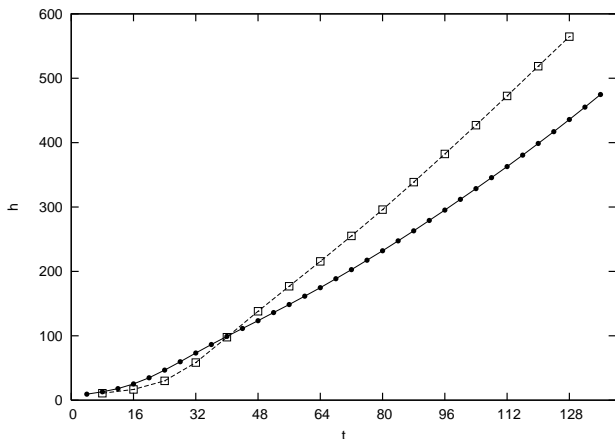


FIG. 3: Mixing widths h in simulations with narrow (solid line) and wide (dashed line) initial spectra.

III. SCALES OF RAYLEIGH-TAYLOR TURBULENCE

A. Mixing zone width

The mixing zone width is the standard characteristic used in the α -studies [9]. According to the most recent analysis [15, 18], the mixing zone width obeys the scaling, $\sqrt{h} = \sqrt{h_0} + t\sqrt{\alpha Ag}$, where h_0 is an initial-conditions-dependent constant. In the simulation with narrow initial spectrum, we reproduce this scaling relatively well; in the faster-developing simulation with a broad initial spectrum the scaling is affected by the finite domain size (Figure 3).

The value of α depends on the definition of the mixing zone width. Following [6, 11, 18] we consider the definition based on the mixing function, $M(c) = 4c(1 - c)$,

$$h = \int M(\bar{c})dz, \quad (3)$$

where the overbar denotes averaging over the horizontal plane. We prefer integral definitions of the mixing zone width over the common definitions based on the values of \bar{c} (for example the half-distance H between two heights where $\bar{c} = 0.01$ and $\bar{c} = 0.99$) simply due to the fact that integral quantities are less sensitive to the profile of $\bar{c}(z)$ at the edges of the mixing layer, and consequently the quantities are less sensitive to the size of the computational domain. In the established self-similar regime unrestricted by domain boundaries, two definitions of the mixing zone width are actually within an $O(1)$ systematic factor of each other. The value of the coefficient α , determined from the slopes of the curves shown in Figure 3 at $t > 60$ are $\alpha = 0.029$ for the narrow initial spectrum and $\alpha = 0.040$ for the broad initial spectrum. The obtained values of α are in a good agreement with other simulations (see reviews in [9, 10]). Experimental values are higher, $\alpha \approx 0.5-0.7$, which is usually attributed to

the presence of longer wavelengths in the initial spectra, and our simulation with broader initial spectrum follows the same tendency. As we show below, in spite of the difference in α , the two systems are very similar. Further broadening of the initial spectrum would require larger and more expensive simulation, while we do not expect the results to be significantly different.

An important thesis of the phenomenology [19] is that the internal structure of the mixing zone senses the overall time scale only adiabatically through slowly evolving large scale characteristics, of which the mixing zone width, h , is the benchmark one. Therefore, our intention is to separate the “large scale” question of the overall time dependence of the mixing zone width from the set of focused “small scale” questions about internal structure of the mixing zone. To achieve this goal, we track the dependence of the various internal characteristics of the mixing zone (see below) on the mixing zone width.

B. Energy-containing scale

The energy-containing scale represents the size of a typical turbulent eddy which, intuitively, corresponds to the size of the large scale vortices seen in the mixing zone snapshot, e.g. shown in Figure 2. Formally, it is convenient to define this scale, R_0 , as the correlation length of the normalized two-point pair correlation function of velocity, $f(R) = \langle v_i(r)v_i(r+R) \rangle / \langle v_i^2 \rangle$, where v_i is one spatial component of the velocity vector, \mathbf{v} . We estimate R_0 as a half width of the correlation function, $f(0)/f(R_0) = 2$. Defined this way, R_0 is consistent (up to some π -dependent constant) with the wavelength (inverse of the wave vector) where the turbulent energy spectra achieves its maximum. See e.g. Figure 11.

In the developed regime, the correlation length taken at the center of the mixing zone grows linearly with the mixing layer width, $R_0 \approx h/30 + 7$ and $R_0 \approx h/17 + 6$ for correlations between horizontal and vertical velocities respectively for both types of initial perturbation (Figure 4). In the limit of large R_0 , this suggests significant separation between the two scales, $h : R_0 = 17 : 1$ or more.

Ristorcelli and Clark [15] introduced their version of the energy containing scale as $L = v_z^3/\epsilon$, and found this scale to be of the order of the width of the mixing layer, $L \approx 0.4h$. Note that defining L requires a single point measurement, while R_0 characterizes the two-point correlations. This single-point nature of L makes it the preferred large scale characteristic in the engineering closure modeling. Our simulations show that L is significantly larger than R_0 , where both L and R_0 scale linearly with h : $L \approx 7 - 15R_0 \approx 0.5h$. The scale separation of L and R_0 may be viewed as a very favorable fact for the engineering modeling of the RTT, thus suggesting a numerical justification for the closure schemes, e.g. of the type discussed in [15].

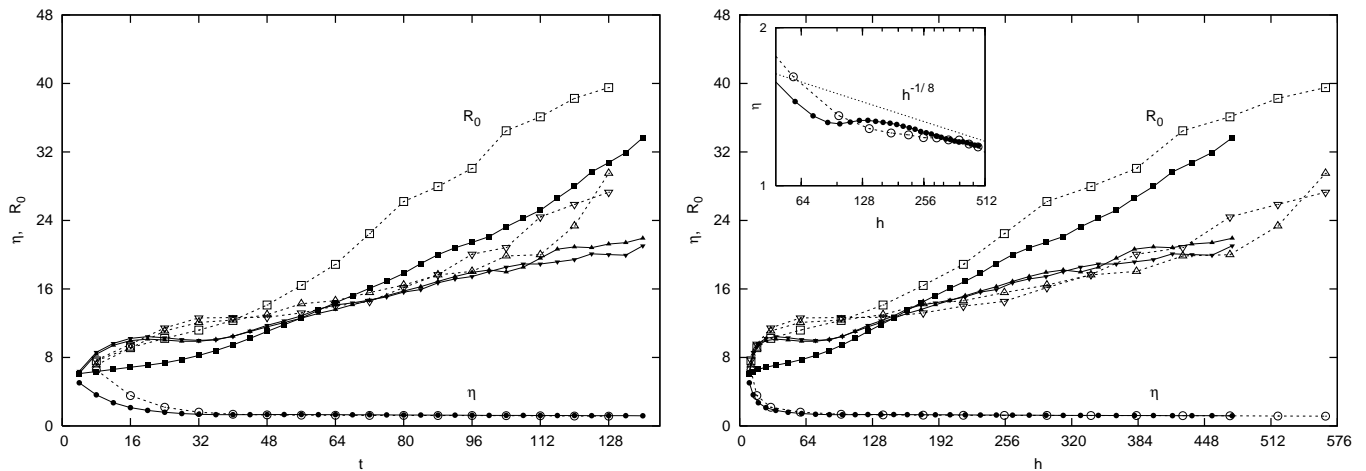


FIG. 4: The energy containing scale (correlation length) and the viscous scale in the middle of mixing layer in the simulations with narrow (solid line) and broad (dashed line) initial spectra. Squares and triangles correspond to scales computed using vertical and horizontal components of the velocity, respectively.

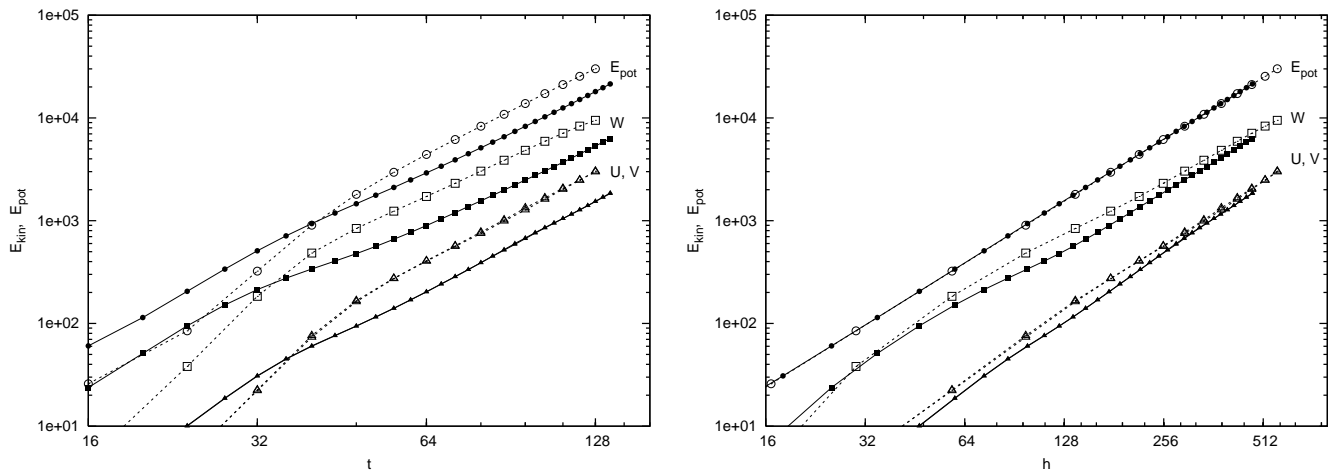


FIG. 5: Released potential energy and components of the kinetic energy integrated across the mixing layer in simulations with narrow (solid line) and broad (dashed line) initial spectra.

C. Viscous and dissipation scales

In our simulations $\kappa = \nu$, thus the viscous scale and the dissipation scale are equal to each other. (This simplification reflects our desire to focus on the larger scale physics while keeping the resolution domain sufficiently large.) We estimate the viscous scale in the middle of the mixing layer ($z = 0$) directly as $\eta \sim (\nu^3/\epsilon)^{1/4} \sim (\nu^2/\langle 5(\nabla v)^2 \rangle)^{1/4}$. (The “5”-factor here is an artifact of an old tradition, see e.g. [25].) In magnitude, the viscous scale agrees with [18] and with the respective phenomenology estimate [15, 19], $\eta \sim ((\nu/v)^3 h)^{1/4}$. The viscous scale decreases slowly with time (see Figure 4). However, our data are too noisy to claim anything more than rough consistency with the $h^{-1/8}$ predicted in [15, 19] and observed in [15, 18].

D. Relative dependence of scales

In view of our focus on the internal structure of the mixing zone, we choose to study the relative dependence of the relevant scales. Thus, Figure 6 shows dependence of the energy-containing and viscous scales on the mixing zone width.

Analyzing simulations of RTT corresponding to different initial perturbations, we confirm the earlier observed [14, 15] sensitivity of time-evolution of the mixing zone width, scales η and R_0 , and the integral quantities on initial conditions. (See left panels in Figures 4 and 5.) However, we also find that the same quantities re-plotted as functions of h look very much alike (Figures 4 and 5, right panels). Therefore, one conclusion we draw here is that the relative scale representation is actually a better universal indicator of turbulence within the mixing zone.

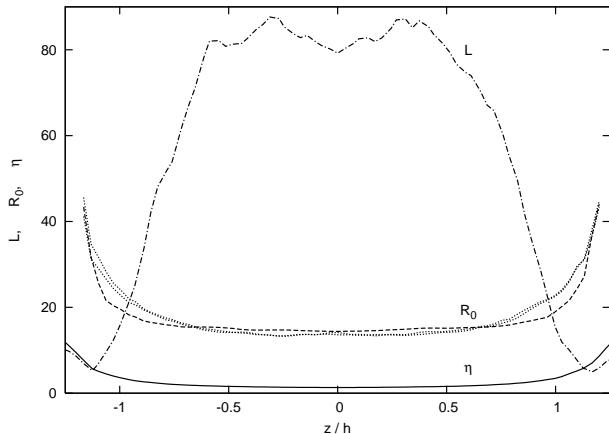


FIG. 6: R_0 – energy containing scale based on the two-point correlation function, L – energy containing scale based on the single point measurements (see discussion in the text for details), and η – the viscous scale, all plotted at time $t = 64$ in simulations with narrow initial spectrum as functions of the distance from the middle of the mixing layer. Dashed and dotted lines correspond to scale R_0 computed using vertical and horizontal components of velocity respectively.

IV. STRUCTURE OF THE MIXING LAYER

A. Self-similarity

Figure 7 shows dependencies of the mixing function and of the RMS-averaged velocities across the mixing layer on the height, z . In magnitude, the velocities are $O(h^{1/2})$, as suggested by the h^2 -dependence of the total kinetic energy: $E \sim v^2 h$ (See Figure 5). The curves taken at three different times are almost indistinguishable from each other. This suggests that the mixing zone, viewed from the large-scale perspectives, is self-similar.

Self-similarity of the averaged density and the averaged velocities was observed in [10, 13, 14, 15, 16, 17]. The self-similarity itself does not define the specific form of the z -averaged profiles, only suggesting that these profiles are smooth functions of z/h . In particular, self-similarity is in principle consistent with specific parabolic predictions for the size of the dominant eddy and total kinetic energy contained in the mixing layer [17, 26], $K(z) = K_0(1 - z^2/h^2)$ and $L(z) = L_0\sqrt{1 - z^2/h^2}$, where K_0 and L_0 are respective characteristics measured in the middle of the mixing layer. Notice, however, that our simulation results, shown in Fig. 6, suggest a much flatter profile for kinetic energy than the parabolic one.

We notice that when illustrating self-similarity (see for instance [15]), it is common to rescale the mean profiles of different quantities using the values at the center of the mixing layer and plot these profiles as function of z/h . Here, we propose to use h -based scalings not only for the z -coordinate but also for the discussed quantity. Thus, in Figure 7 we rescale velocities with \sqrt{h} .

In addition to the mixing function dependence on z ,

Figure 7 shows $1 - \theta(z) = 1 - \overline{M(c)}/M(\bar{c})$ to be almost constant inside of the mixing layer, with a sharp drop-off near the edges. Profiles of $\theta(x)$, sometimes called the molecular mixing fraction, were obtained experimentally and numerically in [6, 8, 9, 10, 27], and most of the observations agree on the fact that at the later stages of the RT instability $\theta(x)$ remains constant across the mixing layer at approximately 0.75-0.8. This suggests that a θ -based definition of the mixing zone width can be advantageous because it generates a more robust scaling.

The h -scaling and self-similarity of the mean profiles are also observed in the probability distribution functions (PDFs) as well as in the correlation functions for density and velocities computed at $z = 0$ (see Figures 8 and 9). The self-similarity is observed at sufficiently large times, $t > 64$, but is lacking at the earlier times (not shown in the Figures). The dynamics one sees at the earlier times for the PDF points to transition from a single peak curve to two peaks and to a single peak again. The explanation for this phenomenon is as follows. The initial, single peak distribution is dependent on the initial perturbation of the originally sharp interface. The transformation from one to two peaks corresponds to transition to the non-linear regime of the RT instability, associated with the secondary Kelvin-Helmholtz type shear instability and the formation of RT mushrooms. The transition from two peaks to one corresponds to the destruction of RT mushrooms and formation of the turbulent mixed zone. Notice that the emergence of the earlier time transitions is consistent with results reported in [6, 10, 16] for the PDF of density, where, probably, the asymptotic self-similar regime was not reached yet.

B. Dependence of scales on z -location

A discussion of scales is rare in the existing literature, not to mention a discussion of how the scales vary across the mixing zone. This is partly due to difficulties with experimental diagnostics. Notable exceptions are [15] and [17], which discuss the energy containing scale within simulations and one-dimensional modeling, respectively. The model in [17] predicts a parabolic profile for the energy containing scale, and this appears consistent with earlier time observations in [15] and in our setting. At later stages the profile in [15] changes to a much flatter one, which also agrees with our estimates of the energy containing scale based (as in [15]) on single point measurements. Moreover, we show that later in time these profiles stabilize in a nontrivial self-similar solution (Figure 10).

Our measurements, based on the two-point correlation functions of density and velocities as well as estimates of the dissipation scale η , also exhibit monotonic dependence on z/h . As shown in Figure 6, both R_0 and η vary insignificantly across the mixing layer with a slight increase towards the edges. Among the scales we measured, R_0 is the only scale which the self-similarity in

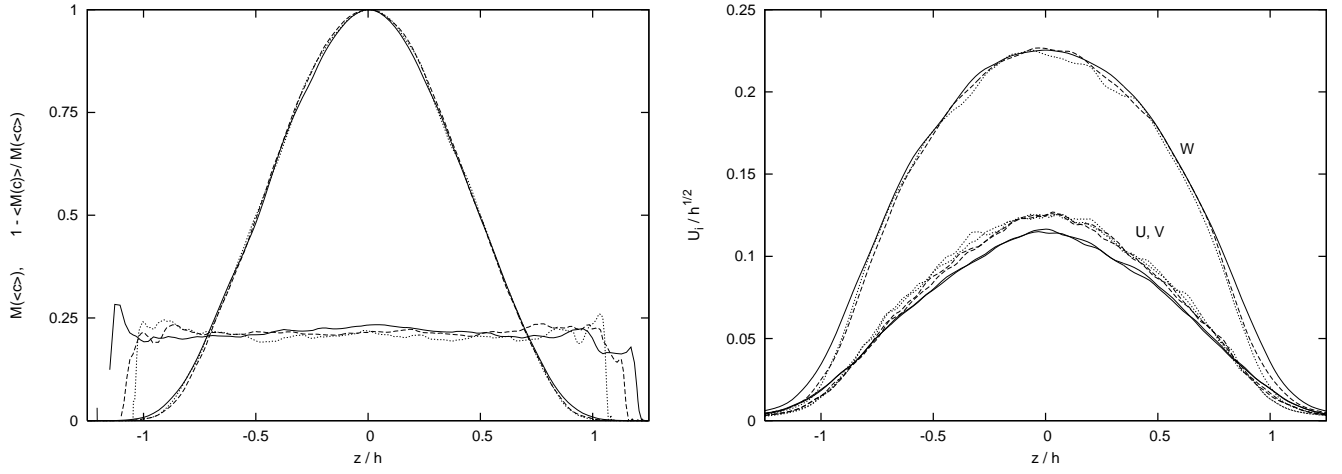


FIG. 7: Mixing function (left) and velocities (right) vs distance from the center of the mixing layer. The quantities are shown at times $t = 64$ (solid line), $t = 96$ (dashed line), and $t = 128$ (dotted line) for narrow initial spectrum.

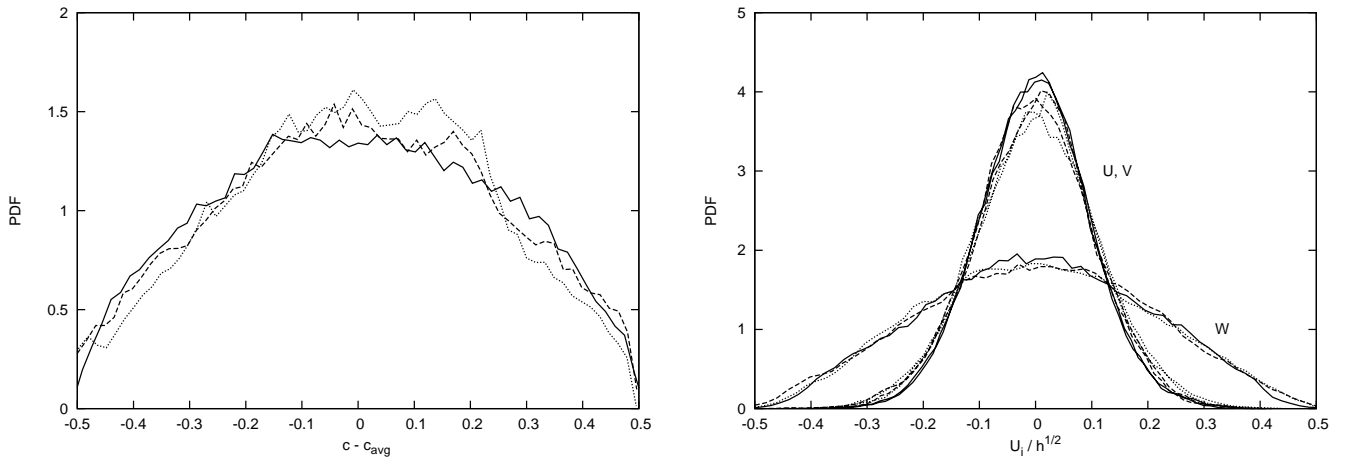


FIG. 8: PDF of density (left) and velocities (right) in the center of the mixing layer at times $t = 64$ (solid line), $t = 96$ (dashed line), and $t = 128$ (dotted line) for narrow initial spectrum.

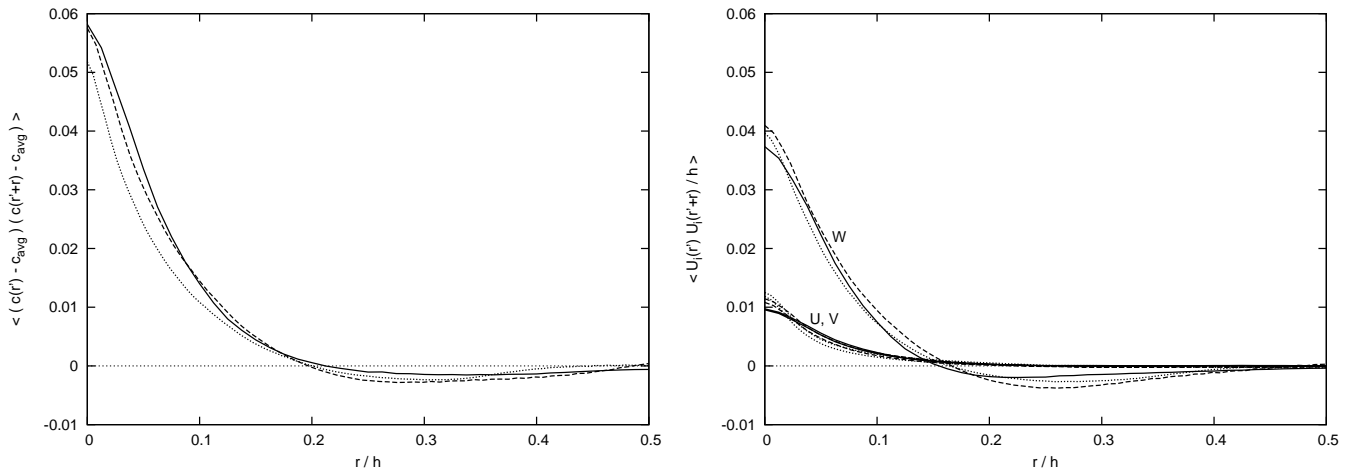


FIG. 9: Correlation functions of density (left) and velocities (right) in the center of the mixing layer at times $t = 64$ (solid line), $t = 96$ (dashed line), and $t = 128$ (dotted line) for narrow initial spectrum.

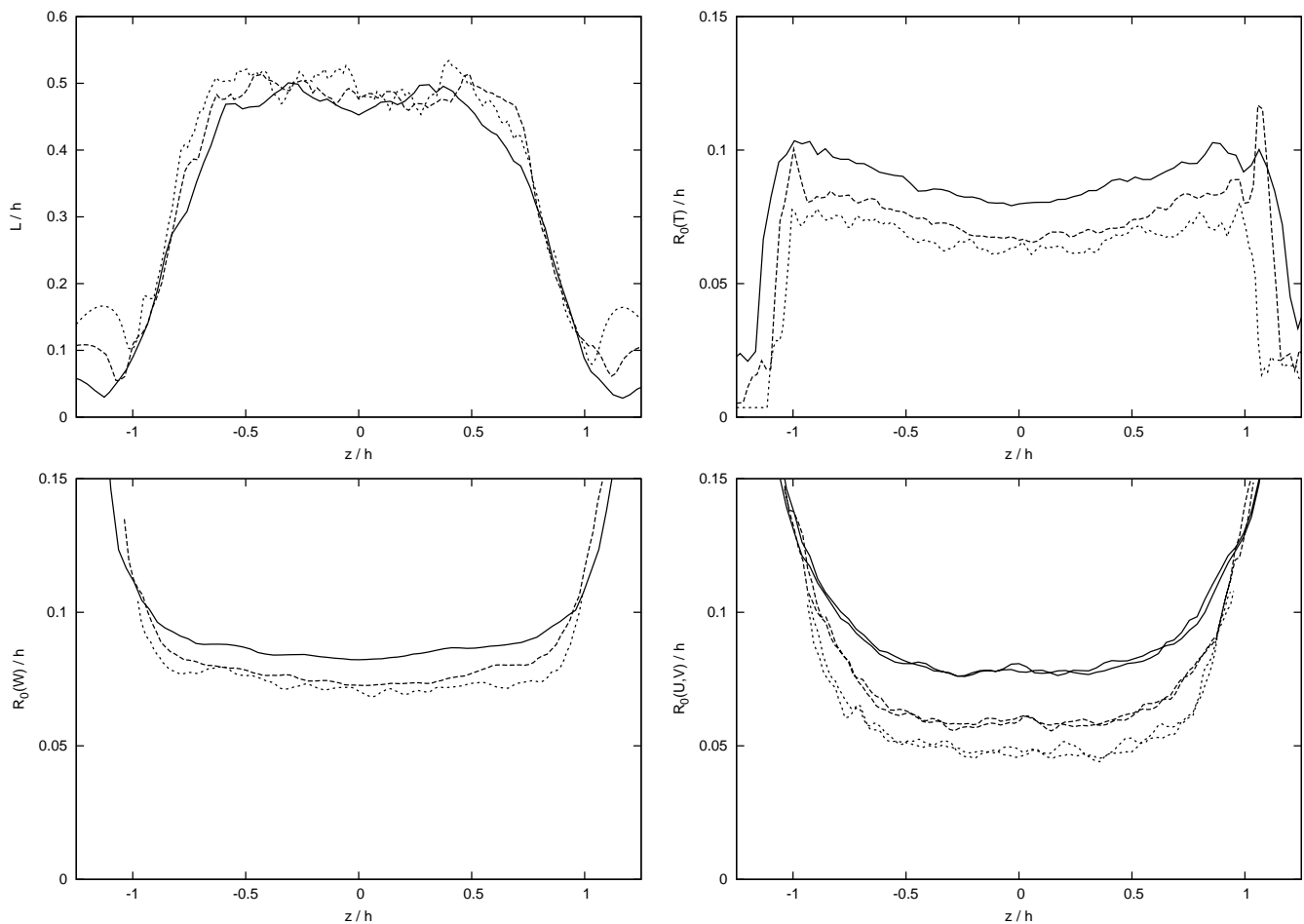


FIG. 10: The energy containing scale based on the single point measurements, L , and based on the two-point correlations of density and velocities, R_0 , as function of the distance from the center of the mixing layer at times $t = 64$ (solid line), $t = 96$ (dashed line), and $t = 128$ (dotted line) for narrow initial spectrum.

time is still questionable (Figure 10). It might be related to a resolution-related systematic error in obtaining the correlation functions near zero (Figure 9).

Comparing the respective curves for different initial spectra, we find that the dependence of $R_0(z/h)$ and $\eta(z/h)$ on initial perturbation is weak.

C. Energy spectra

As expected the level of fluctuations grows with time, resulting in a monotonic shift of the turbulence spectra maxima towards larger wavelengths. The energy-containing wavelength, λ_0 , (corresponding to the maximum) is in agreement with the correlation radius, R_0 . This applies to various spectra. For example, the maximum of the W^2 -spectrum obtained at $z = 0$ and $t = 64$, and shown in Figure 11 (right), is located at $k \approx 0.15$, i.e. $\lambda \approx 42$. The correlation radius at this time is $R_0 \approx 14 \sim \lambda/\pi\sqrt{2}$. At time $t = 124$ the spectrum maximum shifts to $k = 0.07$ ($\lambda \approx 90$) while $R_0 \approx 30$.

Extracting the Kolmogorov scaling for velocity fluctuations at different wavelengths as well as the largest wavelength cutoff (corresponding to the inverse of the viscous scale) from the spectral data (e.g. Figure 11) is problematic due to the lack of spatial resolution. In this regard our simulations, as well as many others, e.g. [6, 9, 14, 16], lack the power of the simulations performed by Cook and Cabot [16, 18]: the latter provide the only reliable confirmation (so far) of the expected Kolmogorov features of the spectra. (These record simulations are an LES run [16] and a DNS run with 3096^3 points resolution [18].) Based on our simulation results, we can only state that the range of scales compatible with the Kolmogorov scaling grows with time and that the viscous scale decreases with time in accordance with predictions of [15, 19].

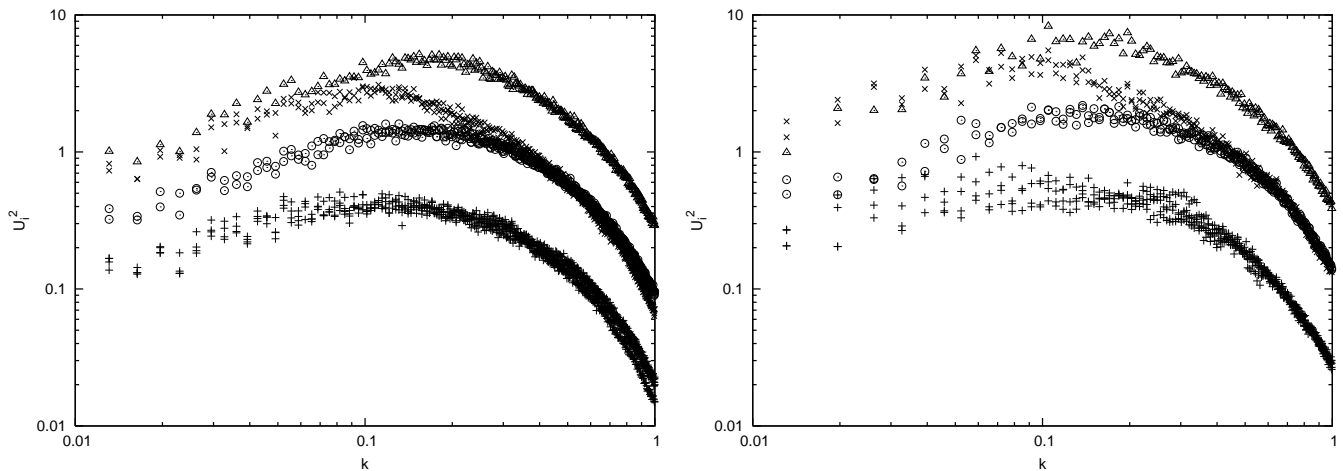


FIG. 11: Energy spectra at time $h \approx 180$ in horizontal planes $z = 0$ (circles - horizontal velocities, triangles - vertical velocities) and $z \pm 0.75h$ (+ horizontal velocities, \times vertical velocities) in simulations with narrow (left) and broad (right) initial spectra.

V. CONCLUSIONS

We conclude by presenting a question-and-answer style summary for the observations made in the article.

- *Does the relative dependence of the characteristic scales constitute a better indicator of self-similarity within the RTT than the dependence of the individual scales on time?* We found that the energy-containing scale, R_0 , and the viscous scale, η , exhibit monotonic evolution with h . At transient times both R_0 and η demonstrate much clearer scaling with h than with the observation time t .
- *How does the energy containing scale, R_0 , compare with h ?* We found that at late time, the ratio of R_0 to h taken at the center of the mixing zone is $\approx 1 : 20$ and fluctuates little with time.
- *Do the turbulent spectra vary with vertical position of the mixing zone?* Analyzing spatial correlations for a given time snapshot, we did not observe any qualitatively new features of the turbulence spectra

with transition from the vertically central slice to an off-centered one within the mixing zone.

- *How different are the scales and the spectra corresponding to qualitatively different initial perturbations?* We found that the dependencies of R_0 and η , as functions of z/h , on the initial perturbations are weak.

Our effort to extend this type of analysis to account for the effects of chemical reactions on the RT Boussinesq turbulence will be described in a forthcoming article [28].

Acknowledgments

We wish to thank P. Fischer for the permission to use the Nekton code, A. Obabko and P. Fischer for the detailed help in using the code, and J.R. Ristorcelli for useful comments. This work was supported by the U.S. Department of Energy at Los Alamos National Laboratory under Contract No. DE-AC52-06NA25396 and under Grant No. B341495 to the Center for Astrophysical Thermonuclear Flashes at the University of Chicago.

-
- [1] Rayleigh, Lord, "Investigation of the character of the equilibrium on an incompressible heavy fluid of variable density," Proc. of the London Math. Soc. **14**, 170 (1883).
 - [2] G. Taylor, Taylor, Sir Geoffrey Ingram, "The instability of liquid surfaces when accelerated in a direction perpendicular to their planes," Proc. of the Royal Soc. of London. Series A, Mathematical and Physical Sciences, **A201**, No. 1065, 192 - 196 (1950).
 - [3] S. Chandrasekhar, *Hydrodynamic and hydrodynamic instability*, Dover Publications, NY 1961.
 - [4] R. E. Duff, F. H. Harlow, C. W. Hirt, "Effects of diffusion on interface instability between gases," Phys. Fluids **5**, 417 (1962).
 - [5] D. H. Sharp, "An overview of Rayleigh-Taylor instability," Physica D **12**, 3 (1984).
 - [6] S. B. Dalziel, P. F. Linden, and D. L. Youngs, "Self-similarity and internal structure of turbulence induced by Rayleigh-Taylor instability," J. Fluid Mech. **399**, 1 (1999).
 - [7] D. L. Youngs, "Numerical simulation of turbulent mixing by Rayleigh-Taylor and Richtmyer-Meshkov instabilities," Laser and Particle Beams, **12**, 725 (1994).
 - [8] P. F. Linden, J. M. Redondo, D. L. Youngs, "Molecular mixing in Rayleigh-Taylor instability," J. Fluid. Mech. **265**, 97 (1994).
 - [9] G. Dimonte et al, "A comparative study of the turbulent

- Rayleigh-Taylor instability using high-resolution three-dimensional numerical simulations: The Alpha-Group collaboration,” *Phys. Fluids* **16**, 1668 (2004).
- [10] P. Ramaprabhu and M. J. Andrews, “Experimental investigation of Rayleigh-Taylor mixing at small Atwood numbers,” *J. Fluid. Mech.* **502**, 233-271, (2004).
- [11] M. J. Andrews and D. B. Spalding, “A Simple Experiment to Investigate Two-Dimensional Mixing by Rayleigh-Taylor Instability,” *Phys. Fluids A* **2**, 922-927, (1990).
- [12] P. N. Wilson and M. J. Andrews, “Spectral measurements of Rayleigh-Taylor mixing at small Atwood number,” *Phys. Fluids* **14**, 938 (2002).
- [13] Y. N. Young, H. Tufo, A. Dubey, and R. Rosner, “On the miscible Rayleigh-Taylor instability: two and three dimensions,” *J. Fluid Mech.* **447**, 377 (2001).
- [14] A. W. Cook and P. E. Dimotakis, “Transition stages of Rayleigh-Taylor instability between miscible fluids,” *J. Fluid Mech.* **443**, 69 (2001).
- [15] J. R. Ristorcelli and T. T. Clark, “Rayleigh Taylor turbulence: self-similar analysis and direct numerical simulation,” *J. Fluid Mech.* **507**, 213 (2004).
- [16] A. W. Cook, W. Cabot and P. L. Miller, “The mixing transition in Rayleigh-Taylor instability,” *J. Fluid. Mech.* **511**, 333 (2004).
- [17] G. Dimonte and R. Tipton, “K-L turbulence model for the self-similar growth of the Rayleigh-Taylor and Richtmyer-Meshkov instabilities,” *Phys. Fluids* **18**, 085101 (2006)
- [18] W. H. Cabot and A. W. Cook, “Reynolds number effects on Rayleigh-Taylor instability with possible implications for typeIa-supernovae,” *Nature Physics* **2**, 562 (2006).
- [19] M. Chertkov, “Phenomenology of Rayleigh-Taylor Turbulence,” *Phys. Rev. Lett.* **91**, 115001 (2003).
- [20] A. N. Kolmogorov, “The equation of turbulent motion in an incompressible viscous fluid”, *Izv.Akad. Nauk. SSSR, Ser.Fiz.* **VI**(1-2), 56 (1941).
- [21] A. Celani, A. Mazzino, and L. Vozella, “Rayleigh-Taylor turbulence in two dimensions”, *Phys. Rev. Lett.* **96**, 134504 (2006).
- [22] M. Zingale et al, “Three-dimensional numerical simulations of Rayleigh-Taylor unstable flames in Type Ia supernovae,” *Astrophysical Journal* **632**, 1021 (2005).
- [23] P. F. Fischer, G. W. Kruse, and F. Loth, “Spectral element methods for transitional flows in complex geometries,” *J. of Sci. Comput.* **17**, 81-98 (2002)
- [24] P. Ramaprabhu, G. Dimonte, and M.J. Andrews, “A numerical study of the influence of initial perturbations on the turbulent Rayleigh-Taylor instability,” *J. Fluid Mech.* **536**, 285 (2005).
- [25] H. Tennekes, J. L. Lumley, *First course in turbulence*, MIT Press, 1972.
- [26] D. M. Snider and M. J. Andrews, “The Simulation of Mixing Layers Driven by Compound Buoyancy and Shear,” *ASME Journal of Fluids Engineering*, **118**, 370-376 (1996).
- [27] D. L. Youngs, “Three-dimensional numerical simulation of turbulent mixing by Rayleigh-Taylor instability”, *Phys. Fluids A* **3**, 1312 (1991)
- [28] M. Chertkov, V. Lebedev, and N. Vladimirova, “Reactive Rayleigh-Taylor Turbulence” submitted to *J. Fluid. Mech.*, <http://arxiv.org/abs/0807.3772>, LANL Preprint: LA-UR-07-7260
- [29] In two dimensions RTT is markedly different from its three dimensional counterpart: buoyancy and inertia effects are in balance, resulting in the so-called Bolgiano-Obukhov scaling regime. The *2d* phenomenological prediction of [19] was numerically confirmed in [21].